Glacier Mass Balance Studies on Gangju La Glacier (2024-2025)

Cryosphere Services Division
National Center for Hydrology and Meteorology
2025

List of acronyms:

- MSI – Multispectral Instrument
- RTK – Real-Time Kinematic
- GNSS – Global Navigation Satellite System
- mm w.e. a^{-1} – Millimeter Water Equivalent per Annum
- DEM – Digital Elevation Model
- IDW – Inverse Distance Weighting
- AGMB – Annual Glacier Mass Balance
- CGMB – Cumulative Glacier Mass Balance
- TCS7 – Trimble Controller Series 7
- WGS 84 – World Geodetic System 1984
- CSV – Comma-Separated Values
- Gt – Gigatonnes
- m.a.s.l. – meters above sea level

Executive Summary

Gangju La Glacier was assessed for the 2024–2025 glaciological year under Bhutan's benchmark glacier monitoring program, and the results confirm continued glacier mass loss, frontal recession, and measurable areal shrinkage. The area averaged annual specific mass balance was estimated as −1613.876 mm w.e. a^{-1}, indicating substantial net thinning over the observation period, with the true value expected to fall within the stated uncertainty range. Consistent with the point mass-balance profile, the equilibrium-line altitude (ELA) was estimated to lie above the glacier surface during the survey periods (ELA ≈ 5281.5 m a.s.l. in 2024 and 5480.8 m a.s.l. in 2025), indicating an ablation-dominated regime across the observed elevation range. In addition to the mass loss, the glacier terminus retreated by 11.86 m, showing that the negative mass balance is also expressed as frontal shrinkage. Consistent with these changes, glacier area has decreased from 0.237 km^2 (2017) to 0.169 km^2 (2025), representing a net loss of 0.068 km^2 (~28.7%) over the period. The spatial pattern of surface change indicates thinning is widespread and generally stronger at lower elevations, while surface lowering decreases toward higher elevations, consistent with elevation-dependent melt processes on clean-ice Himalayan glaciers.

The uncertainty (±236.482 mm w.e. a^{-1}) reflects the combined effects of the main error sources in the geodetic workflow, including variability in elevation-band mass-balance estimates, uncertainty in glacier boundary delineation that influences hypsometry and area-weighting, and uncertainty related to the density assumptions used to convert elevation change to water equivalent. Together, these findings provide a robust, uncertainty-bounded estimate of annual glacier change for Gangju La, while the documented longer-term area reduction (2017–2025) reinforces evidence of sustained glacier recession, strengthening Bhutan's long-term cryosphere record and supporting downstream water-resource and hazard assessments.

Table of Contents

List of Figures

Table

1.Introduction

Bhutan, situated in the eastern Himalaya, contains ~700 glaciers with a total mapped area of 629.55 km² (BGI, 2018). As part of the High Mountain Asia (HMA) cryosphere, Bhutanese glaciers contribute to "mountain water tower" functions that support downstream water supply and energy systems, while also influencing the exposure of communities and infrastructure to cryosphere-related hazards (Immerzeel et al., 2020). In Bhutan, these linkages are particularly relevant because seasonal snow and glacier melt modulate headwater discharge that underpins irrigation, domestic supply, and hydropower development.

Across the globe, glacier mass loss has accelerated under anthropogenic warming. A recent intercomparison synthesis estimates a mean global glacier mass loss of 273 ± 16 Gt yr^{-1} during 2000–2023, with a significant increase after 2012 (The GlaMBIE Team, 2025). Independent global assessments based on multi-mission geodetic elevation change similarly indicate sustained, widespread glacier thinning in the early 21st century (Hugonnet et al., 2021). Within HMA, regional geodetic studies show broadly negative mass balances during the satellite era (Brun et al., 2017; Shean et al., 2020). Specifically for the eastern Himalaya centred on the Bhutan–China border, declassified satellite imagery and modern DEM differencing reveal significant ice loss since the 1970s, demonstrating that long-term thinning is not restricted to the western Himalaya (Maurer et al., 2016).

Beyond static thinning and terminus retreat, glacier–lake interactions can amplify mass loss by triggering dynamic thinning and flow acceleration. This mechanism has been explicitly documented in Bhutan, where land- to lake-terminating transitions have been linked to speed-up and enhanced surface lowering (Sato et al., 2022). In parallel, glacier-lake evolution can elevate downstream hazard potential through GLOF processes; recent basin-scale analyses in the Pho Chhu system quantify flood scenarios and downstream impacts for major lakes in Bhutan (Wangchuk et al., 2024). These coupled changes underscore the need for consistent monitoring that connects glacier mass change to both hydrological implications and hazard assessment.

Long-term in situ mass-balance series remain sparse in the Bhutan Himalaya and across HMA, yet they are essential for (i) attributing observed glacier changes, (ii) constraining geodetic mass-balance estimates derived from remote sensing, and (iii) reducing uncertainty in regional projections (Brun et al., 2017; Shean et al., 2020; The GlaMBIE Team, 2025). Gangju La

Glacier (≈0.17 km²; 4,800–5,200 m a.s.l.), located in the headwaters of the Pho Chhu, is one of Bhutan's benchmark glaciers for sustained mass-balance monitoring. In situ observations began in 2003, providing the first multi-year, field-based mass-balance record for the Bhutan Himalaya (Tshering and Fujita, 2016). That record reported persistently negative annual balances over 2003–2014 and indicated an equilibrium-line altitude above the glacier surface, implying net ablation over the entire glacier during that period (Tshering and Fujita, 2016).

In this study, we present the area-averaged mass balance of Gangju La Glacier for the glaciological year 2024–2025. Using an in situ geodetic approach, we quantify area averaged net balance (mm w.e.), estimate mass change, and compute terminus recession. The results strengthen Bhutan's benchmark glacier time series and provide empirically grounded information to support regional hydrological assessments, climate-impact evaluation, and cryosphere hazard monitoring in the eastern Himalaya.

2.Aim and Objective

The primary aim of this study is to assess recent changes in the mass balance and terminus position through in-situ based geodetic method, thereby contributing to Bhutan's long-term glacier monitoring and climate adaptation efforts.

3.Study Area

3.1 Location

A clean type Gangju La Glacier is located in WGS 84/UTM zone 45N of Bhutan at 27.94°N, 89.95°E (Figure 1) with an approximate area of 0.169 km². It extends from an elevation of 4900 to 5200 m.a.s.l., referred to as "PPhgr16_189" in an inventory compiled by the National Center for Hydrology and Meteorology (NCHM, 2018).

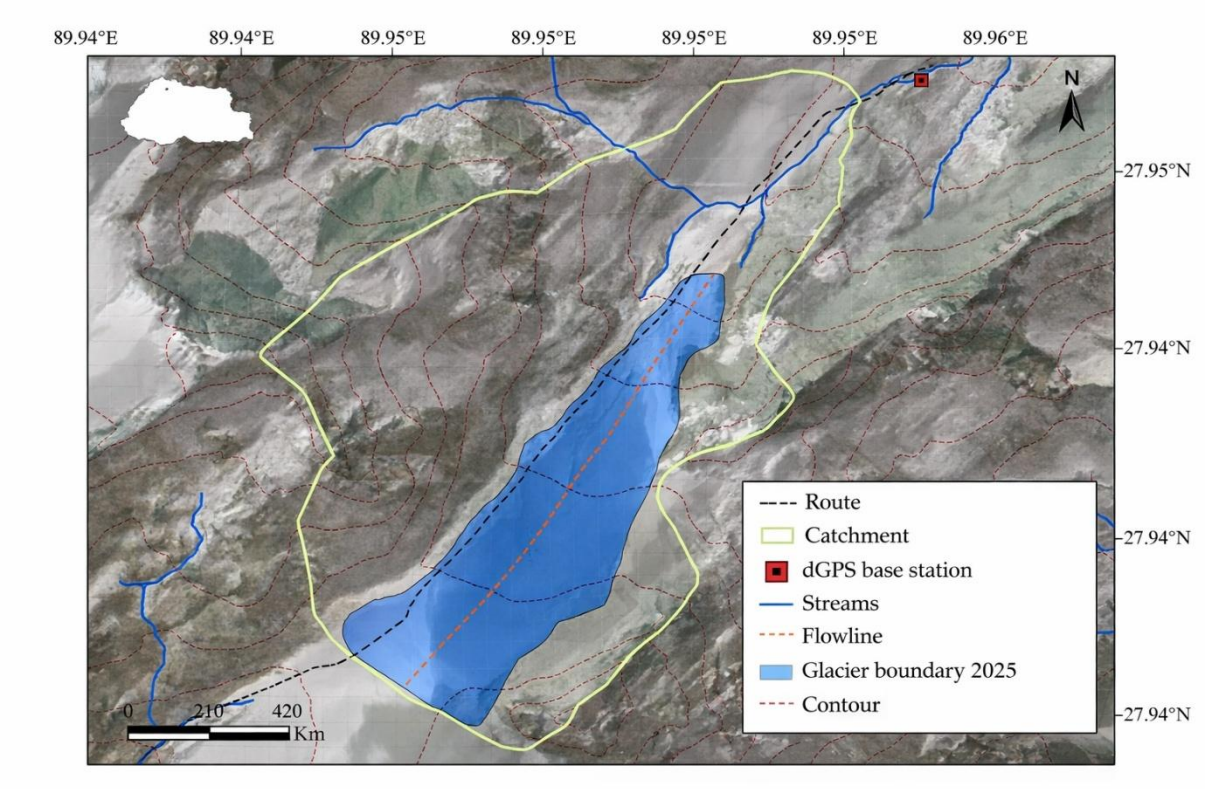

Figure 1: Location of Gangju La Glacier at the headwaters of the Pho Chhu, within the Punatsang Chhu Basin. Basemap is a median Sentinel-2 true-color composite (September–November 2025) draped over a hillshade (70% transparency).

3.2 Accessibility

This route can be accessed via two options. The first route is via Gasa-Laya-Tarina-Gangju La, which takes seven days on foot. The other route is via Ramina-Gangju La and takes five days to reach the study site. It is en route to Lunana Gewog of Gasa Dzongkhag.

4. Data and Methodology

4.1 Data Acquisition

Gangju La Glacier is located en route to Lunana Gewog of Gasa Dzongkhag. It is challenging to collect data using direct methods because of human disturbances. Therefore, the monitoring team relies on only in-situ geodetic methods to continuously monitor this glacier. During the field expedition, glacier surface elevation data were collected using RTK GNSS (Trimble R10-2). Prior to the survey, Trimble R10-2 was calibrated for higher precision to avoid errors. The base station was set up accurately on the previously marked point (reference point), which is at a certain distance away from the glacier snout and kept at the height of 2m from the ground. Manually inserting the known coordinate of base station in TCS7 controller of Trimble R10-2, base station was set to start for the collection of data. A rover was mounted on a backpack and

the height of the rover from the ground was measured and entered in the controller accordingly. The logging distance of 1m with a logging interval of one second was set for all survey profiles in continuous Topo mode. Glacier surface elevations data were collected by walking across the glacier following the survey track file (shape file) of the previous year. Several new points were collected for future reference. Similarly, glacier terminus data were collected by walking on the glacier, following the snout of the glacier for that given point of time. Unlike glacier surface elevations, there is no reference to previous year's data to walk through it. Glacier terminus either advances or recede-in most cases they recede. Therefore, a profile along the current terminus position is taken by walking along the terminus of the glacier and compared with the previous terminus profile line to determine the changes in terminus position of the glacier.

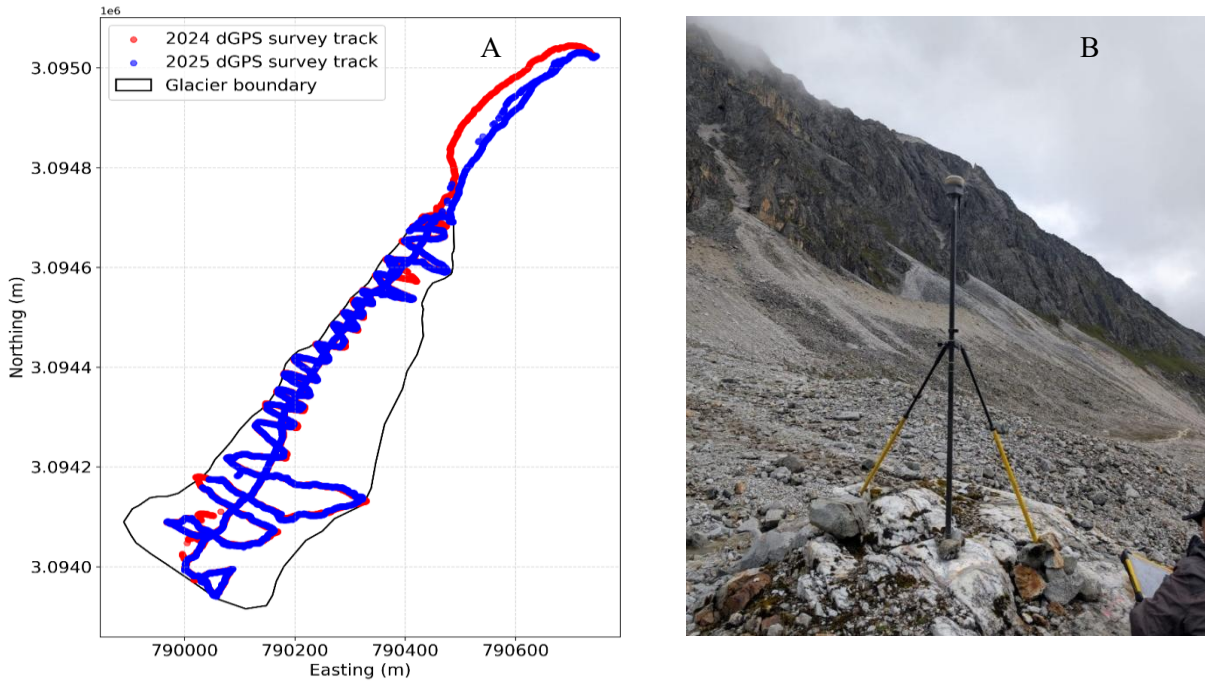

Figure 2: A) dGPS survey tracks. B) Base set up.

4.2 Data Post Processing

4.2.1 Overview of approach

The flowchart provides an overview of the workflow used to derive area averaged mass balance using an in-situ geodetic approach. It combines the surface elevation difference between the previous year (t1) and the current year (t2) from dGPS surveys with DEM bias correction, glacier hypsometry, and snow-depth modelling, followed by area-weighted integration and uncertainty assessment to estimate area averaged mass balance. All the

calculations closely follow established geodetic mass-balance concepts applied in the first in-situ record of decadal glacier mass balance (2003-2014) from the Bhutan Himalaya study by Tshering and Fujita (2016).

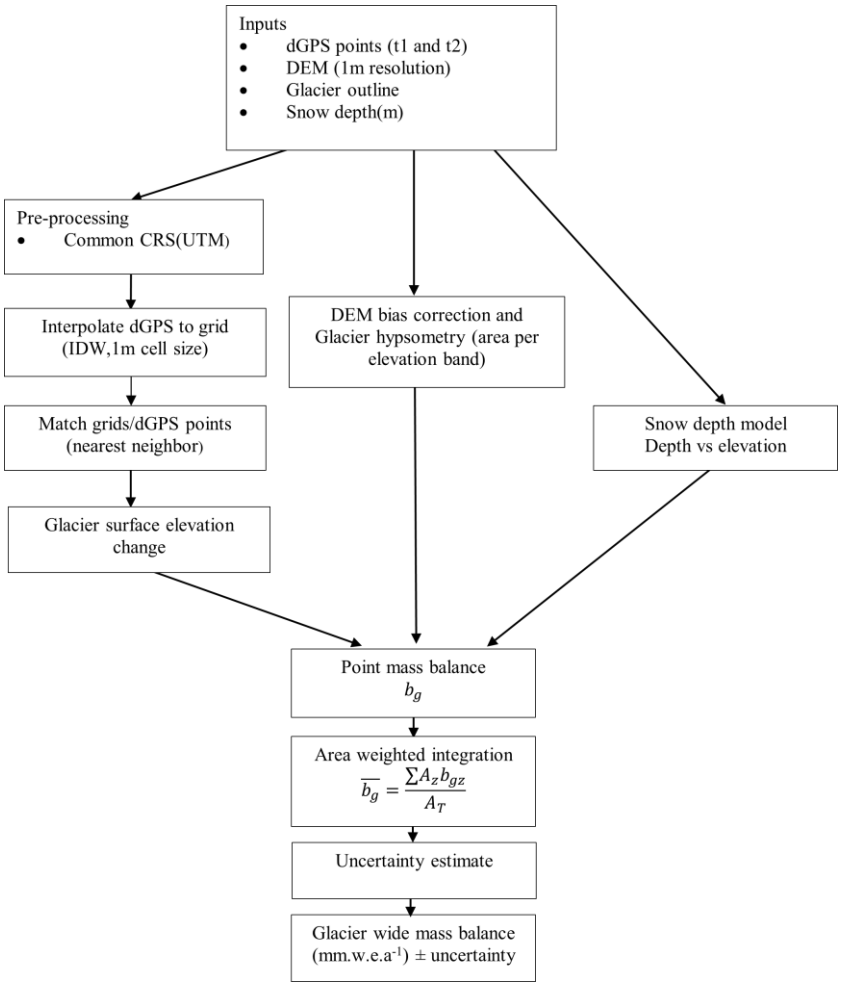

Figure 3: Workflow for glacier mass balance measurement.

4.2.2 Datasets and inputs

Glacier surface elevations measured using dGPS surveys acquired at two years, representing time period 1 (t1: previous year) and time period 2 (t2: current year) were treated as direct observations of the glacier surface elevation at the time of each survey and were used as the primary input for estimating surface elevation change between the two periods.

DEM and glacier outline

To delineate the glacier boundary, a recent Sentinel-2 median composite image (2025; 10 m resolution) was used, and the glacier outline was manually digitized in QGIS. Field-based dGPS glacier surface elevation points were then used for quality control and to apply a vertical bias correction to the 1 m DEM (Maxar) acquired a few years earlier. The corrected DEM, clipped to the mapped glacier extent using the glacier outline polygon, was subsequently used

to derive glacier hypsometry (area distribution by elevation bands) and to ensure all terrain analyses were restricted to the glacier area.

Snow depth

Snow depth information and an elevation obtained at the mass balance stakes collected on two survey dates were used to estimate the snow thickness at a mid-elevation of every 50m elevation band.

Software and processing environment

Remote sensing data preparation and geospatial preprocessing were carried out using a combination of cloud-based and desktop GIS tools alongside Python. A Sentinel-2 median composite (2025; 10 m) was extracted using Google Earth Engine (GEE) to support glacier boundary identification. The glacier outline was then manually delineated in QGIS, which was also used for study area mapping. Subsequent data processing and analysis were implemented in Python using standard scientific and geospatial libraries. Numerical computation and tabular data handling were performed with NumPy and Pandas, while figures and plots were produced using Matplotlib. Vector geospatial operations (e.g., handling glacier outlines, point geometries, and spatial joins) were carried out using GeoPandas, with Shapely used for geometry construction and manipulation. Raster-based DEM processing, including reading and masking/clipping to the glacier boundary, was conducted using Rasterio (including rasterio.mask). Robust trend fitting for elevation-dependent modelling (e.g., Δh–elevation relationships) was implemented using TheilSenRegressor from scikit-learn.

4.2.3. Pre-processing and quality control

All input dGPS survey files were first imported from CSV format and checked to ensure the required coordinate and elevation fields (x, y, z) were present. The coordinate and elevation values were then converted to numeric format, and any records containing missing, non-finite, or otherwise invalid values (e.g., NaN) were removed to prevent errors in subsequent processing. Prior to any spatial analysis, all datasets and spatial layers were verified to be referenced in a common coordinate system (UTM Zone 45N) to ensure positional consistency during interpolation, clipping, and overlay operations. Finally, unit consistency was enforced across the workflow, with both horizontal coordinates and vertical elevations expressed in meters, ensuring compatibility between dGPS measurements, DEM data, and derived outputs.

4.2.4 Interpolation of dGPS points onto a 1 m grid (IDW)

To enable consistent spatial pairing between survey periods and support elevation differencing,

the irregularly spaced dGPS surface elevation points were interpolated onto a regular 1 m grid using Inverse Distance Weighting (IDW). Prior to interpolation, the dGPS coordinates and elevations (x, y, z) were validated by converting values to numeric type and removing any records containing missing or non-finite entries to prevent propagation of errors into the gridded product.

4.2.5 Grid definition and neighborhood search

A regular grid was generated in UTM Zone 45N using the minimum and maximum bounds of the cleaned dGPS coordinates. For each grid node, neighboring dGPS observations were identified within a 0.7 m search radius using a cKDTree-based neighborhood query to ensure computationally efficient spatial searches. Grid nodes with no neighbors inside the search radius were retained as no-data during interpolation and excluded from the exported output.

4.2.6 IDW formulation and assumptions

Inverse Distance Weighting (IDW) is based on the spatial autocorrelation assumption that nearby locations are more similar than distant ones. For each grid node, the predicted elevation is computed as a distance-weighted average of surrounding dGPS measurements within a defined local search neighborhood. In this workflow, a search neighborhood was used and only points within a 0.7 m radius contributed to the prediction, which both reflects the expected local continuity of glacier surface elevations at meter-scale.

For a grid node at location x, the interpolated elevation $\hat{z}(x)$is given by:

$$\hat{z}(x) = \frac{\sum_{i=1}^{n} w_i z_i}{\sum_{i=1}^{n} w_i}, w_i = \frac{1}{d_i^p} \quad (1)$$

where $z_i$are observed elevations, $d_i$are distances from the grid node to each neighbor point, and p is the power parameter ($p = 2$ in our study, i.e., inverse-distance-squared weighting). Increasing p causes weights to decay more rapidly with distance, making predictions more strongly influenced by the closest points; conversely, low p values yield smoother surfaces with broader influence from neighbors. If an observation coincides exactly with a grid node ($d_i = 0$), the grid node is assigned that measured value directly, consistent with IDW behaving as an exact interpolator at sample locations.

4.2.7 Co-location of survey periods and elevation change computation (Δh)

To quantify surface elevation change between the two-survey year, the gridded (interpolated)

elevation points from current year ($t2$) were spatially co-located with those from previous year ($t1$) prior to differencing. Co-location was performed using a nearest-neighbor spatial join, where each point in the $t2$ dataset was assigned the geographically closest point from the $t1$ dataset based on planimetric distance in the common projected CRS (UTM Zone 45N). An initial broad search cap (e.g., up to 50 m) can be applied to avoid unmatched points in sparse areas and to ensure that point neighbors are identified; however, the final matched dataset was restricted using a stricter acceptance criterion to maintain positional comparability. Specifically, only pairs satisfying a maximum nearest-neighbor distance of $d_{\text{nearest}} \leq 3$ m were retained for analysis. This distance threshold ensures that elevation change is computed only where both survey year represent nearly the same surface location and reduces the risk of introducing spurious Δh values caused by mismatched terrain, interpolation artifacts, edge effects near the glacier margin, or differences in point density between surveys.

4.2.8 Elevation change at matched points

For each accepted matched pair, the surface elevation change was computed as:

$$\Delta h = h_{t2} - h_{t1} \tag{2}$$

where $h_{t2}$and h_{t1}represent co-located elevations for the current and previous year, respectively.

4.2.9 DEM vertical bias check and correction

To minimize systematic elevation offsets in the reference DEM arising from the time gap between DEM acquisition and the study period, a vertical bias correction was performed prior to hypsometric analysis by directly comparing DEM elevations with field-measured dGPS surface elevations. The DEM was first sampled at the dGPS point coordinates, and the elevation residuals were computed as:

$$\Delta z_{\text{DEM–dGPS}} = z_{\text{DEM}} - z_{\text{dGPS}} \tag{3}$$

A single representative vertical bias was then estimated from these residuals (using the mean difference as a first-order approximation) and applied uniformly across the DEM to obtain a corrected elevation surface;

$$z_{\text{DEM,corr}} = z_{\text{DEM}} - \text{bias}. \tag{4}$$

This correction step reflects the broader requirement in geodetic workflows that DEM-based analyses must account for potential vertical offsets to avoid propagating systematic errors into elevation-change and mass-balance estimates. Figure 4A and 4B show the comparison between the dGPS raw data and the Maxar-derived DEM before and after bias correction.

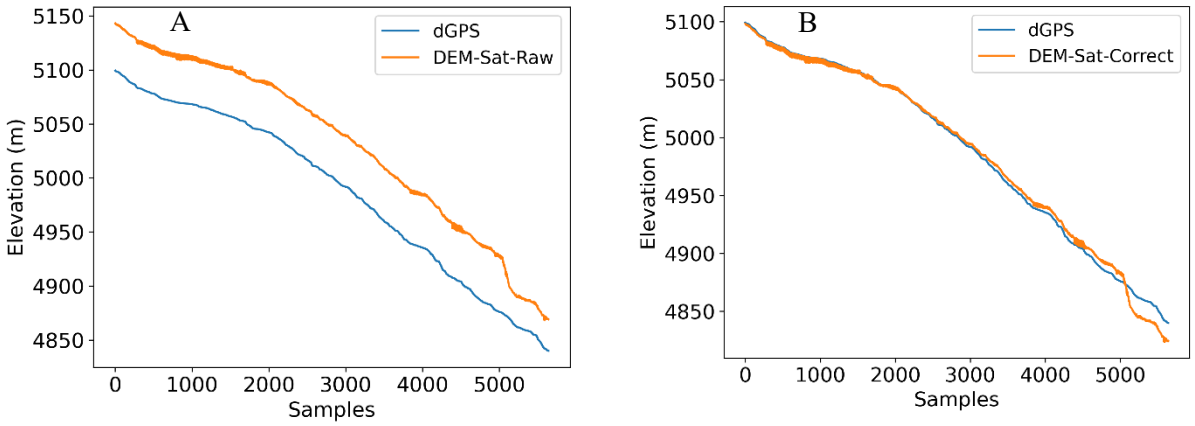

Figure 4: A) Observed difference in the field-based surface elevation and the satellite obtained elevation. B) Bias corrected DEM.

4.2.10 Glacier hypsometry (area–elevation distribution)

Glacier hypsometry (the glacier area distribution with elevation, Figure 5) was derived from the vertically corrected DEM to support elevation-band based integration of mass balance. First, the corrected DEM was clipped using the glacier outline polygon, ensuring that subsequent terrain analysis included only glacier pixels within the mapped boundary. The glacier DEM was then classified into discrete elevation bands using a 50 m interval. For each elevation band z, the glacier area A_z was computed as:

$$A_z = N_z\, r^2 \tag{5}$$

where r is the DEM pixel size in meters and N_z is the number of DEM pixels falling within that band z.

Where glacier extents differed between the two measurement years, the band-wise area was represented using the mean of the two, following Tshering and Fujita (2016). Specifically, for each 50 m elevation band, the representative area was computed as:

$$A_z = (A_{t1} + A_{t2})/2 \tag{6}$$

where $A_{t1}$and $A_{t2}$are the glacier areas (m²) within the same elevation band derived from the outlines corresponding to the surveys at $t1$ and $t2$, respectively. This averaged hypsometry was subsequently used for area-weighted integration of elevation-band mass balance, where $A_z$represents the area in the 50 m band(m²).

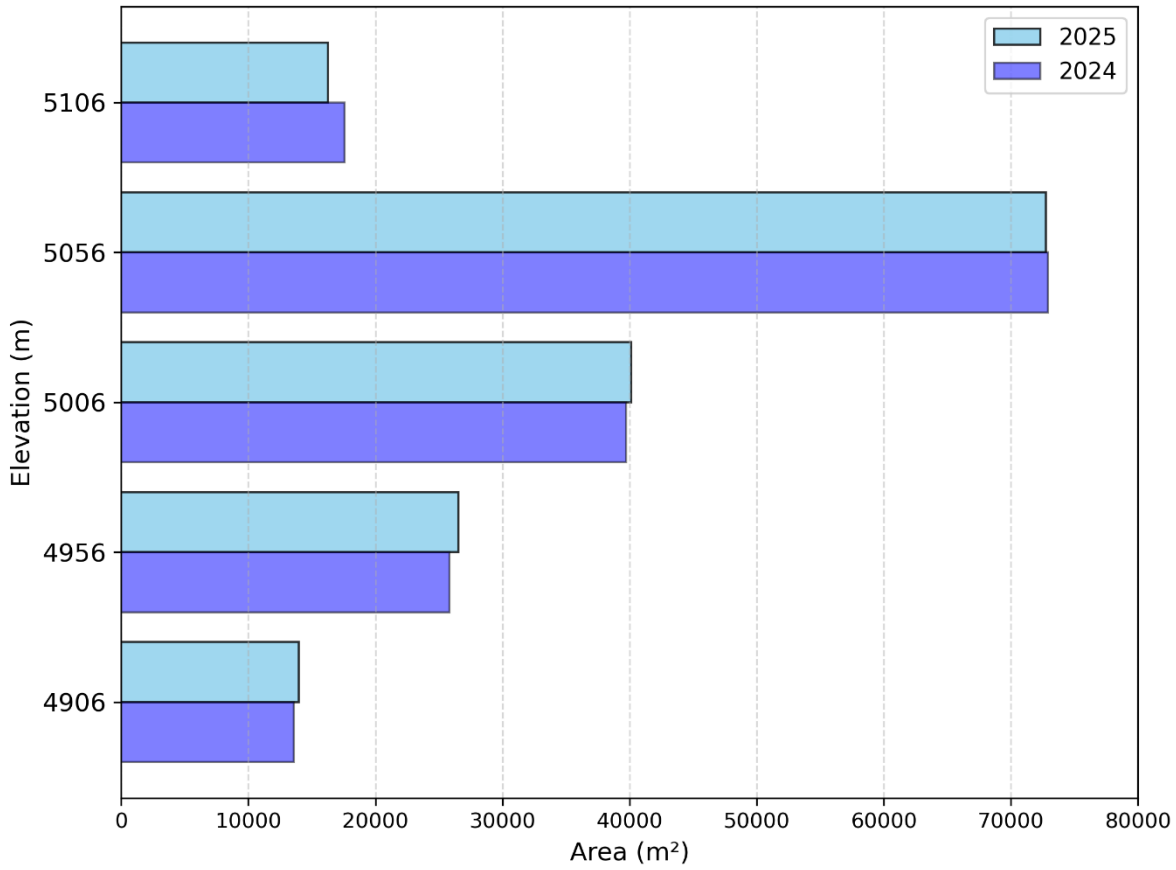

Figure 5:Hypsometry for the year 2024 and 2025

4.2.11 Elevation-band aggregation of Δh and robust smoothing

Following co-location of the two-survey period, the elevation-change observations (Δh) were average by elevation to obtain a stable, hypsometry-compatible representation of surface change across the glacier. Each matched Δh point was assigned to the same 50 m elevation-band scheme used for glacier hypsometry, based on its elevation. For each elevation band, the mean Δh was used as an initial estimate of elevation change within that band. This band-wise aggregation reduces small-scale spatial noise and ensures that elevation change is expressed in a form suitable for subsequent area-weighted integration.

Δh was modelled as a function of elevation using Theil–Sen robust regression (Figure 6), which estimates the trend based on the median of pairwise slopes and is therefore substantially less sensitive to outliers than ordinary least squares regression. The resulting fitted function, $\Delta h(z) \approx f(z)$ was then used to evaluated a missing mean Δh for the mid elevation band, which was used in the subsequent hypsometric integration and mass-balance calculations.

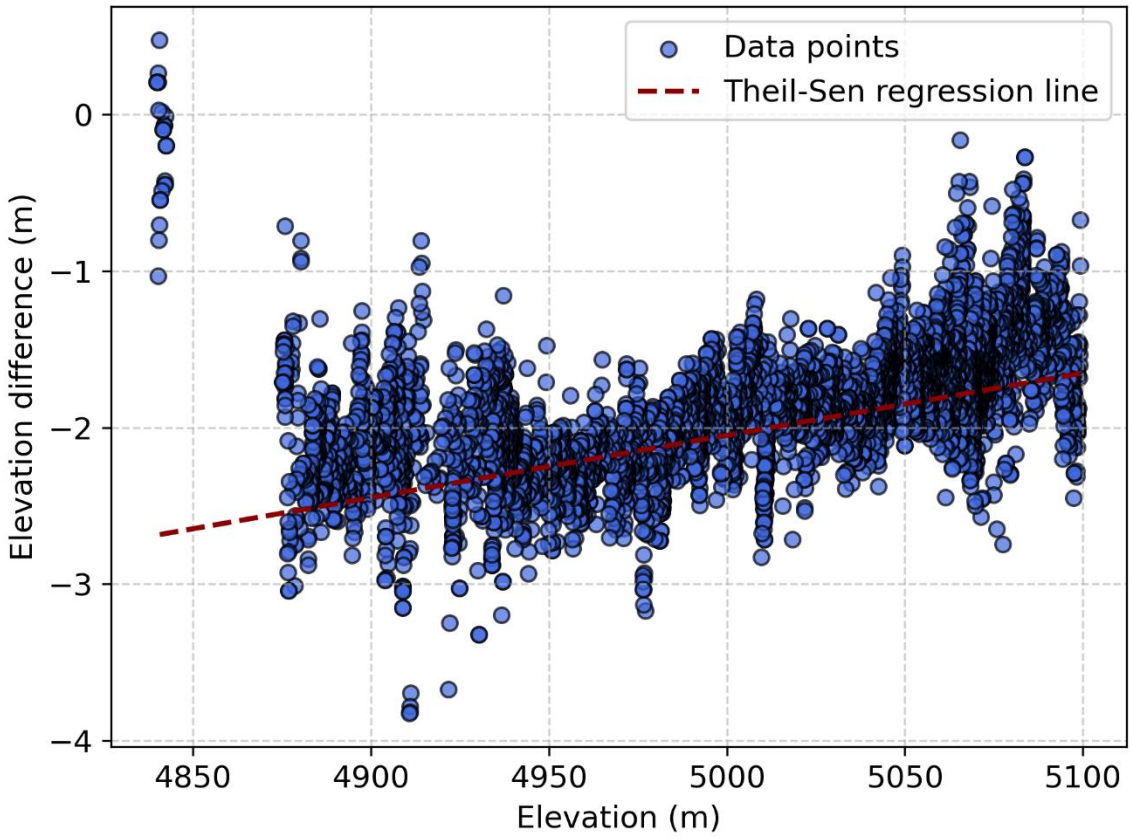

Figure 6:Glacier surface elevation change between 2024 and 2025 generated using dGPS elevation differencing

4.2.12 Snow depth–elevation model and ΔS(z)

Snow depth change (ΔS) can be derived from stake measurements collected on two survey dates and parameterized as a function of elevation so that it can be applied consistently across the same 50 m elevation bands used for hypsometry and elevation-change integration. In such a case, stake observations consist of snow depth (m) and stake elevation (m), and the goal is to estimate representative snow depth at the midpoint of each 50 m elevation band. Snow depth is typically modelled against elevation with the robust approach used for the Δh–elevation relationship, the regression can be fitted using Theil–Sen robust regression to reduce sensitivity to outliers and local variability. The fitted model for each date is then evaluated at each band midpoint to obtain $S_{t1}(z)$and $S_{t2}(z)$, and the band-wise snow depth change is computed as:

$$\Delta S(z) = S_{t2}(z) - S_{t1}(z) \quad (7)$$

However, in the present study period, no seasonal snow cover was observed over the glacier at the time of measurement. Therefore, snow depth correction was not required, and $\Delta S(z)$was assumed to be zero for all elevation bands in the mass-balance calculations.

4.2.13 Conversion to mass balance (point-wise and area averaged)

Geodetic mass balance was derived by converting the mean elevation-change at the mid elevation band into a specific mass-change rate. The workflow first estimates a mid-elevation change for each 50 m elevation band and even predict missing mean Δh, and (where applicable) incorporates a snow-depth term to account for differences between snow and ice density. The resulting point-wise mass balance values are then area-weighted by the glacier's area–elevation distribution to obtain a single area averaged mean mass balance over the period $t_1$to t_2.

Annual mass balance at a point

For each 50 m elevation band z, the point-wise geodetic mass balance was computed using the formulation applied in this workflow:

$$b_{gz} = \frac{\Delta h_g(z)\,\rho_i + (S_{t2}(z) - S_{t1}(z))\,(\rho_s - \rho_i)}{(t_2 - t_1)} \tag{8}$$

where $\Delta h_g(z)$is the mean elevation change for the mid elevation band, $S_{t1}(z)$and $S_{t2}(z)$are the snow depths for each mid elevation band at survey period $t_1$and t_2, and $(t_2 - t_1)$. This expression accounts for the fact that snow-depth changes contribute differently to mass change than ice-thickness changes due to the density contrast between snow and ice. In the present study period, no snow was observed, therefore $(S_{t2} - S_{t1}) \approx 0$and the band-wise equation reduces to:

$$b_{gz} \approx \frac{\Delta h_g(z)\,\rho_i}{(t_2 - t_1)} \tag{9}$$

The above equation yields values in kg m^{-2}; conversion to mm w.e. is described in Annex C.

Area averaged mass balance (area-weighted integration)

The area averaged mean mass balance was calculated by area-weighting the band-wise values using the glacier hypsometry:

$$\overline{b_g} = \frac{\sum_z A_z\ b_{gz}}{A_T} \tag{10}$$

where $A_z$is the glacier area within elevation band z(commonly represented as the mean band area from $t_1$and t_2, i.e., $A_z = (A_{t1} + A_{t2})/2$), and $A_T$is the total glacier area. This hypsometric integration yields a single area averaged mass-balance value representative of the full glacier surface over the observation period.

4.2.14 Terminus Mapping

During the field survey, the glacier terminus was mapped using dGPS by walking along the ice–land boundary at the glacier snout to record a continuous terminus line for the survey year.

Terminus retreat was then calculated along the glacier flow direction by measuring the displacement between the current-year terminus and the reference terminus at multiple locations distributed across the snout. These measurements were taken along several flow-parallel segments, and the resulting retreat distances were averaged to obtain the mean terminus recession for that year.

5. Uncertainty Assessment

5.1 Area averaged mass balance uncertainty

The area-average mass balance estimation is associated with three main uncertainties:

1. Uncertainty in the mass balance at each altitudinal band (db_Z; mm w.e. a^{-1}) is calculated for the bands shown in Figure 8a.

2. Uncertainty from the glacier boundary delineation (dA_Z; m^2), and

3. Uncertainty from the assumed density of ice and snow (db_ρ; mm w.e. a^{-1}).

These uncertainties affect the reliability of the estimated area-average mass balance and are incorporated into the final value as a ± range, indicating possible variation. The combined uncertainty (σ) is calculated following the methodology described in Tshering and Fujita (2016) as:

$$\sigma = \frac{\sum A_Z db_Z + \sum dA_Z |b_Z| + \sum A_Z db_\rho}{A_T} \quad (11)$$

Where:

- A_Z is the area within a 50 m altitudinal band,
- A_T is the total glacier area,
- b_Z is the mass balance at each band, and
- $|b_Z|$ is the absolute mass balance.

The uncertainty from the boundary delineation (dA_Z) is computed as:

dA_Z = 0.5 × pixel resolution × perimeter at each 50 m band

Given the Sentinel-2 MSI image resolution of 10 m, dA_Z is based on half the pixel size (i.e., 5 m) multiplied by the perimeter of the glacier outline at each altitudinal band (Fig.8b).

The uncertainty from the density assumption, db_ρ, arises from variability in the assumed densities of ice and snow. These uncertainties are averaged to represent the overall density-related uncertainty in mass balance estimation. However, no snow was observed during either of the two survey periods; therefore, only ice density uncertainty was considered in the uncertainty analysis. For more details on the rationale behind the uncertainty calculation and the densities assumed, refer to Annex D.

The standard deviation (db_Z) of the mass balance across altitudinal bands, representing the uncertainty from spatial mass balance variation, is calculated as:

$$db_Z = \sqrt{\frac{1}{N}\sum(b_Z - \overline{b_z})^2} \tag{12}$$

Where N is the number of elevation bands and $\overline{b_z}$ is the mean mass balance.

5.2 Uncertainty of mass-balance profile parameters (db/dz and ELA)

In addition to the uncertainty of the area averaged area-average mass balance (Sect. 5.1), uncertainty was quantified for the elevation-dependent mass-balance gradient and the regression-derived ELA. Point mass balances aggregated to 50 m elevation-bin midpoint values were fitted with a linear model $b(z) = az + c$, where $a$is the mass-balance gradient $(db/dz)$and $c$is the intercept. The ELA was derived from the zero-crossing of the fitted profile $(ELA = -c/a)$. Uncertainty in $db/dz$was expressed as a t-based 95% confidence interval from OLS regression $(df = n - 2)$. Because ELA is a ratio of fitted parameters and lies above the observed elevation range (extrapolated), ELA uncertainty was quantified using a non-parametric bootstrap percentile 95% confidence interval (2.5th–97.5th percentiles). Full formulations are provided in Annex A.

6. Results and Discussion

6.1 Area averaged mass balance and uncertainty

The area averaged annual specific mass balance of Gangju La Glacier for the 2024–2025 glaciological year was estimated as −1613.876 ± 236.482 mm w.e.a^{-1}, indicating substantial net mass loss. As illustrated in Figure 7, annual mass balance values are predominantly negative throughout the observation period, and the cumulative mass balance curve shows a persistent downward trend with no indication of stabilization. By 2025, the cumulative mass balance reaches approximately −36876.5 mm w.e., reflecting sustained long-term glacier thinning since the early 2000s. The reported uncertainty (±236.482 mm w.e.a^{-1}) reflects the combined influence of elevation-band variability, glacier boundary delineation, and density assumptions used in the geodetic conversion (Annex A, Table A1), and provides an uncertainty-bounded estimate of recent glacier mass change under prevailing climatic conditions.

The sustained negative mass balance observed at Gangju La is consistent with independent evidence from Bhutan's other benchmark glaciers, indicating a coherent pattern of ongoing glacier mass loss at the national scale. For Thana Glacier, the 2023–2024 assessment reports a cumulative mass balance of −17903.3 mm w.e. a^{-1} (2016-2024), confirming continued net mass loss over the monitoring year. Likewise, Shodug Glacier shows a strongly negative area averaged mass balance in 2024–2025 (geodetic estimate −2791.08 mm w.e. a^{-1}), reinforcing that benchmark glaciers in Bhutan are experiencing persistent net ablation.This pattern aligns with the long-term in situ record from Gangju La presented by Tshering and Fujita (2016), who reported consistently negative annual mass balances on Gangju La over 2003–2014 (approximately −1.12 m w.e. a^{-1}), demonstrating that sustained mass loss has characterised this glacier for at least the last decade-plus. Beyond Bhutan, long-term benchmark observations elsewhere in the HKH similarly indicate persistent negative mass balance: Rikha Samba Glacier (central Himalaya, Nepal) has recorded negative balances in recent observational periods (e.g., −0.39 ± 0.32 m w.e. a^{-1} for 2011–2021) and reanalysed long-term series for Chhota Shigri Glacier (western Himalaya, India) reports negative geodetic mass balances for both 2003–2014 and 2014–2020 and a negative mean over 2002–2023. Although observation periods and methods differ among studies, the consistent sign of mass balance (negative) across Bhutan and the wider HKH supports interpreting Gangju La's measured mass loss as part of a broader, regionally coherent response to recent climate forcing rather than a site-specific anomaly.

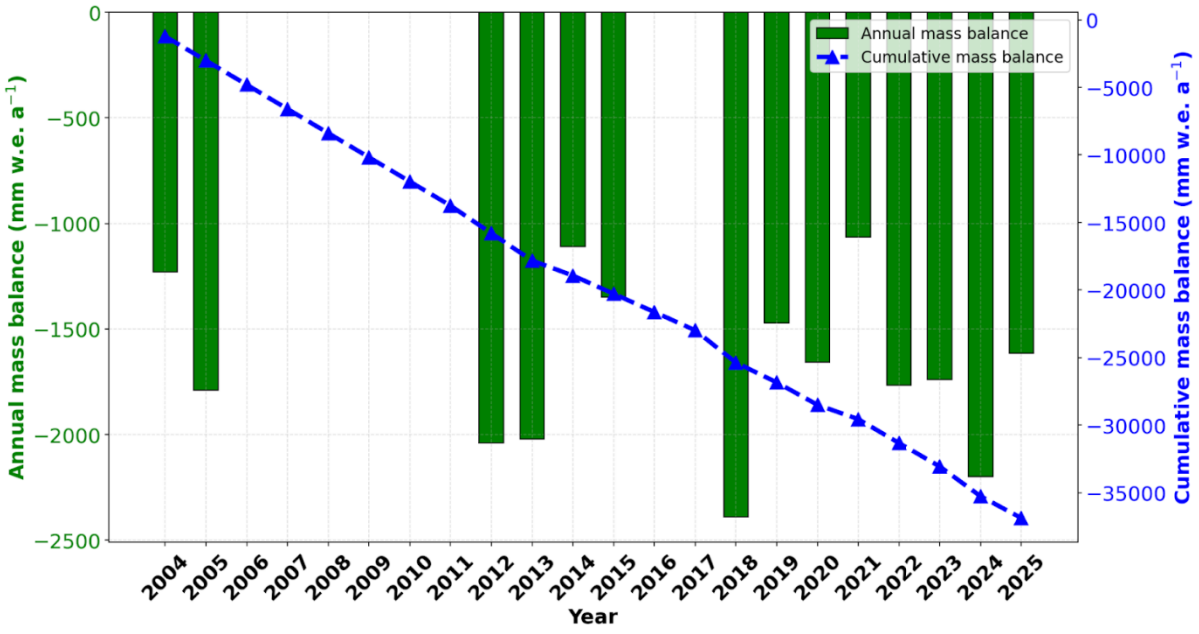

Figure 7:Cumulative mass balance and annual mass balance over the observed periods

6.2 Elevation-dependent surface lowering and hypsometric control

The frequency distribution of elevation differences (Δh) (Figure 8) is centered on negative values, with mean elevation difference of −1.88 m, indicating widespread surface lowering across Gangju La Glacier. Elevation-band analysis (Annex A, Table A1) refines this area averaged signal and shows a clear elevation dependence, with stronger thinning at lower elevations and reduced thinning toward higher elevations: the lowest elevation band (4,881–4,931 m a.s.l.) recorded a mean Δh of −2.17 m, whereas the highest band (5,081–5,131 m a.s.l.) showed a smaller mean Δh of −1.41 m. When integrated hypsometrically, the mid-elevation band (5,031–5,081 m a.s.l.) contributed the largest share (−632.7 mm w.e. a^{-1}) to the area averaged mass balance because it contains the largest fraction of the glacier area (≈43%), demonstrating that the overall mass-balance signal is strongly influenced by the glacier's hypsometry rather than by thinning magnitude alone.

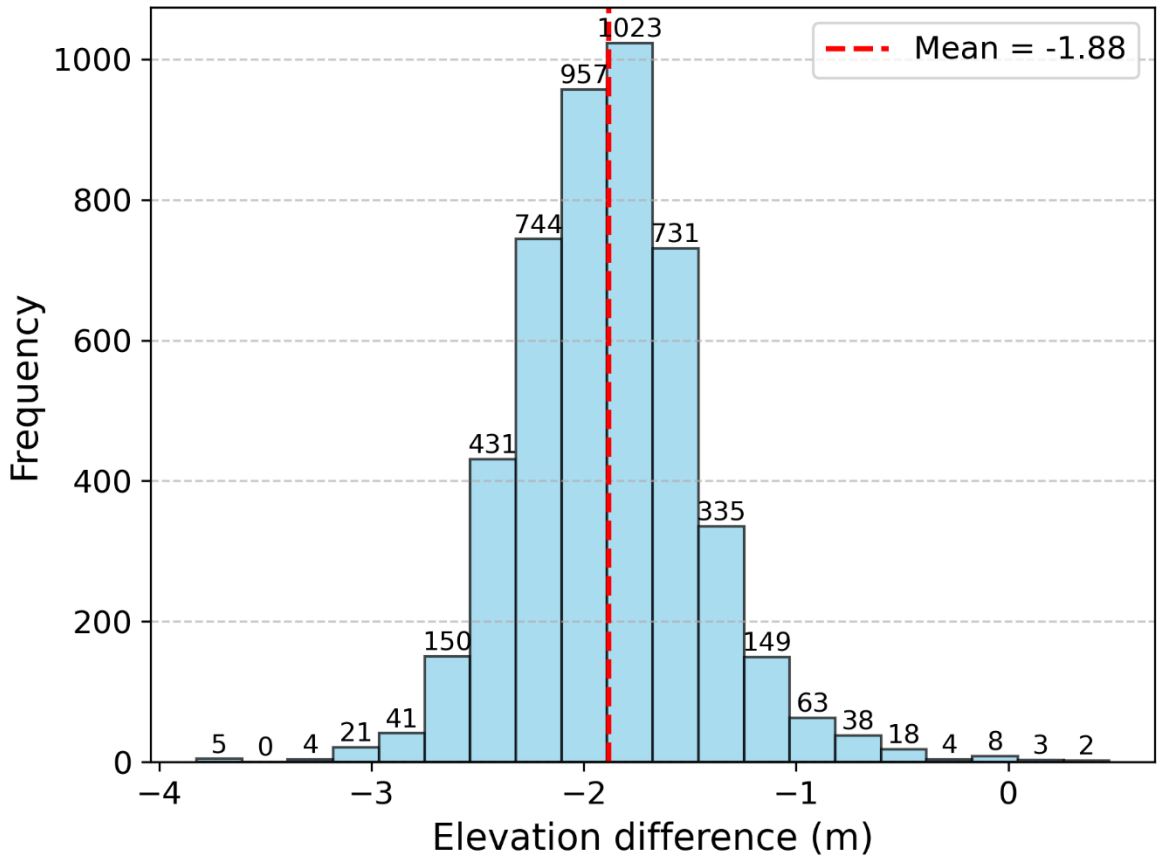

Figure 8:Distribution of glacier surface elevation change between 2024 and 2025.

6.3 Glacier area change

In addition to vertical thinning, Gangju La Glacier has experienced measurable areal changes (Figure 9). Glacier outlines indicate a reduction in surface area from 0.237 km² in 2017 to 0.169 km² in 2025, corresponding to a net loss of 0.068 km² (~28.7%) over the period. The concurrence of surface lowering and area shrinkage reflects a coherent glacier response to sustained negative climatic forcing.

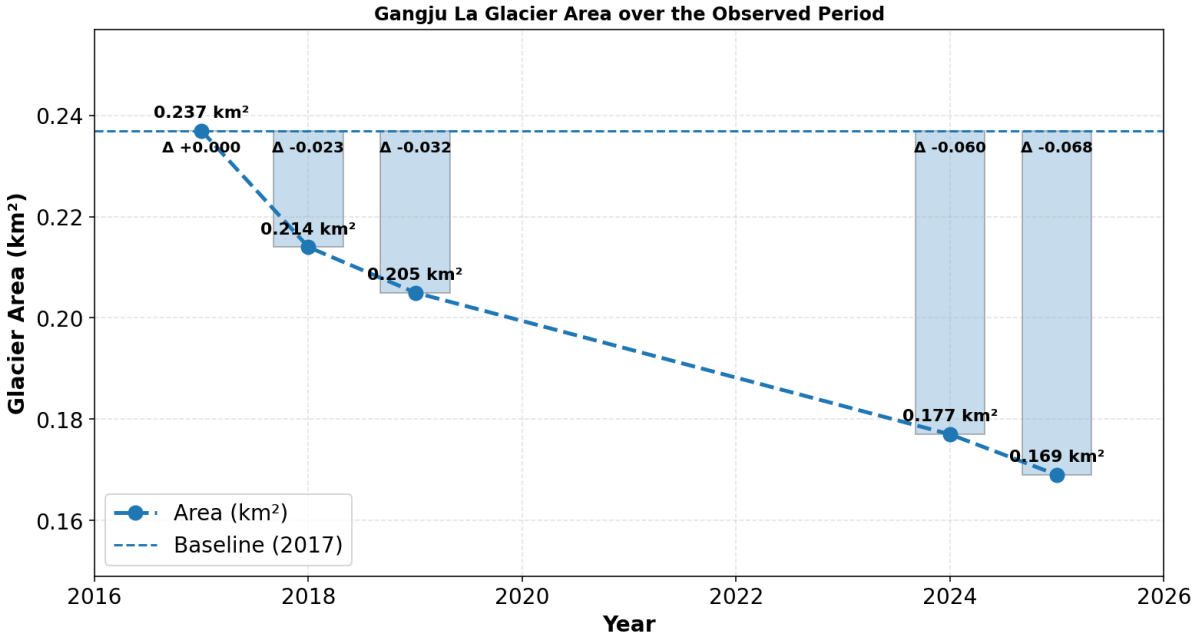

Figure 9: Glacier area for each observation year and the corresponding area change relative to the base year.

6.4 Cumulative terminus recession (2004–2025)

Cumulative changes in glacier length are illustrated by the mapped terminus positions from 2004 to 2025 (Figure 10). Over the past two decades (2004–2024), the glacier terminus retreated by 241.13 m, equivalent to approximately 120.6 m per decade. An additional retreat over most recent survey interval (2024–2025) recorded a mean terminus retreat of 11.86 m, which aligns with the broader cumulative retreat pattern. Together with the observed surface lowering and area reduction, this cumulative terminus recession provides clear visual and geometric evidence of climate-driven glacier change at Gangju La Glacier.

Table 1 summarises mapped terminus retreat for Gangju La Glacier and the resulting cumulative change in glacier length from 2004 to 2025. The record indicates a total cumulative retreat of 252.99 m by 2025, demonstrating persistent frontal recession over the observation period. Retreat is highly variable through time, with several pronounced retreat episodes and years of relatively limited change. The largest displacement is reported for 2014 (106.08 m); this value represents the net terminus change between the 2004 and 2014 mapped positions and therefore reflects the cumulative retreat over that multi-year interval rather than an annual rate. Subsequent retreat continues at a lower but non-uniform magnitude, including notable retreats in 2017 (43.10 m) and 2024 (38.74 m). In contrast, smaller retreat magnitudes occur in years

such as 2021 (2.71 m), illustrating short-term variability superimposed on the long-term recession trend.

Overall, Table 1 provides a consistent geometric indicator of ongoing glacier adjustment and supports the broader evidence of glacier change at Gangju La Glacier derived from area and surface-elevation analyses.

Comparable frontal recession has been documented for other monitored glaciers in Bhutan, indicating that the sustained terminus retreat observed at Gangju La is not an isolated signal. In Bhutan, the national benchmark-glacier assessment reports continued retreat at both Shodug and Thana glaciers, with Shodug retreating by ~15.07 m (2024-2025) and Thana retreated by 30.7 m (2023-2024), confirming persistent recession across Bhutan.

Table 1:Terminus Retreat Over Time

Sl.No	Year	Terminus Retreat (m)	Cumulative Terminus Retreat (m)
1	2004	0	0
2	2014	106.08	106.08
3	2017	43.1	149.18
4	2018	13.7	162.88
5	2019	9.6	172.48
6	2020	12.78	185.26
7	2021	2.71	187.97
8	2022	8.97	196.94
9	2023	5.45	202.39
10	2024	38.74	241.13
11	2025	11.86	252.99

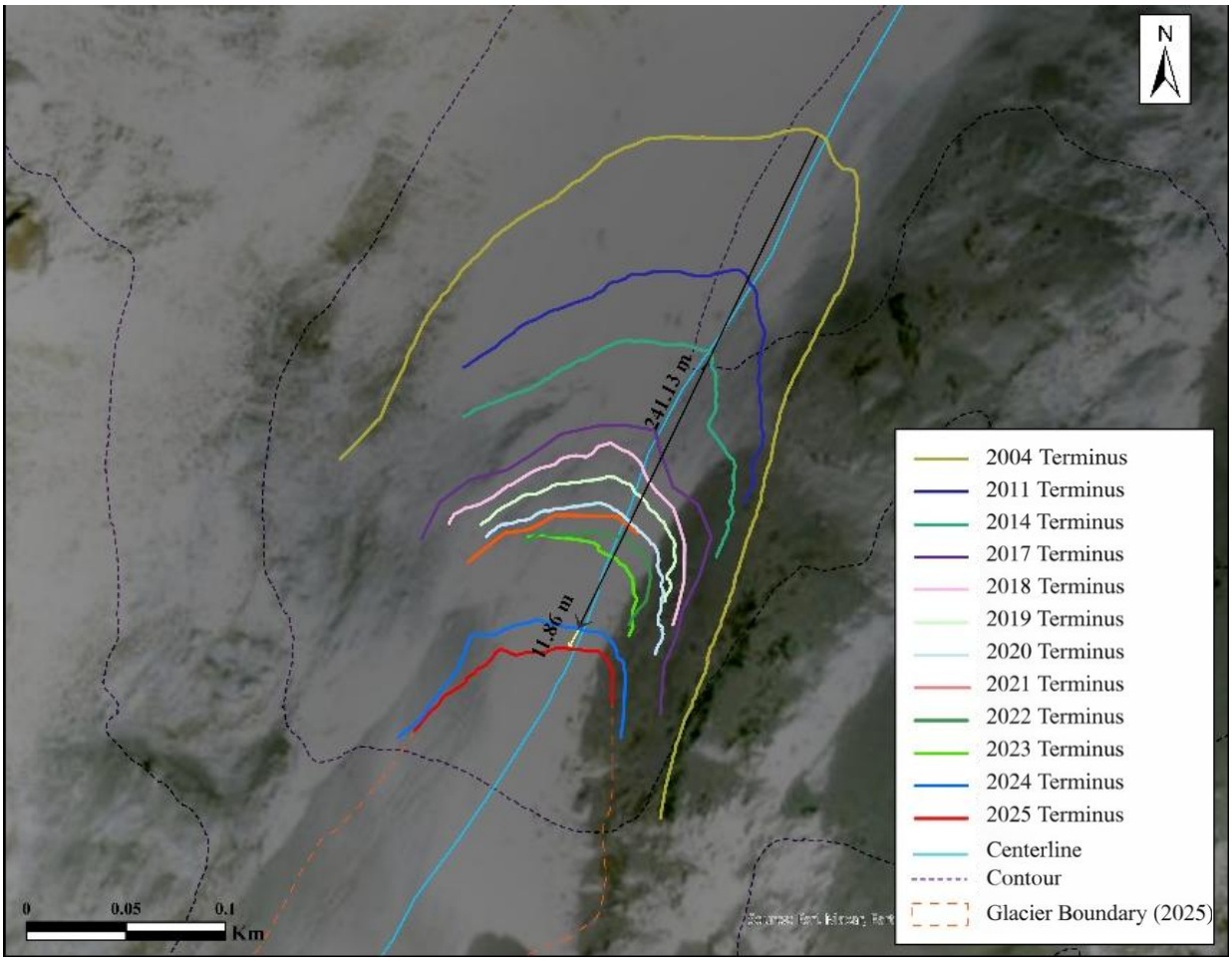

Figure 10:Cumulative terminus positions of Gangju La Glacier from 2004 to 2025. Colored polylines represent mapped terminus locations for individual years; the central flowline is shown for reference. The progressive upstream displacement of the terminus outlines

6.5 Mass-balance gradient and ELA interpretation (2024–2025)

The mass-balance profile derived from elevation-band point observations indicates a robust elevation control on glacier mass balance in both 2024 and 2025 (Figure 11). All band balances within the analyzed elevation range (50 m bands; midpoints 4925–5125 m a.s.l.) are negative in both years, demonstrating net mass loss across the entire sampled zone and implying that the equilibrium line lay above the glacier extent during the survey periods. Linear regression of point/band mass balance as a function of elevation, $b_{gz}(z) = az + c$, shows a strong, approximately linear relationship in both years (2024: $R^2 = 0.960$; 2025: $R^2 = 0.911$). The derived mass-balance gradient in 2024 is $db/dz = 9.65$ mm w.e. m^{-1} (0.965 m w.e. per 100 m; 95% CI: 0.604–1.326 m w.e. per 100 m), whereas in 2025 it decreases to $db/dz = 3.63$ mm w.e. m^{-1} (0.363 m w.e. per 100 m; 95% CI: 0.155–0.572 m w.e. per 100 m). The non-overlapping confidence intervals support a robust weakening of elevation sensitivity in 2025 relative to 2024. A lower gradient indicates that increasing elevation provided less

compensation toward zero balance, consistent with more pervasive ablation extending to higher elevations (e.g., enhanced melt energy and/or reduced albedo protection). The equilibrium line altitude (ELA) estimated from the zero-crossing of the fitted profiles ($b_{gz} = 0$) is 5281.5 m a.s.l. in 2024 (bootstrap 95% CI: 5208–5372 m) and 5480.8 m a.s.l. in 2025 (bootstrap 95% CI: 5379–5895 m), corresponding to an upward shift of ~199 m in 2025. In both years, the ELA lies above the glacier surface extent, consistent with negative balances at all observed elevations and indicating an ablation-dominated regime for the survey periods, in agreement with earlier in situ observations from Gangju La Glacier (Tshering & Fujita, 2016).

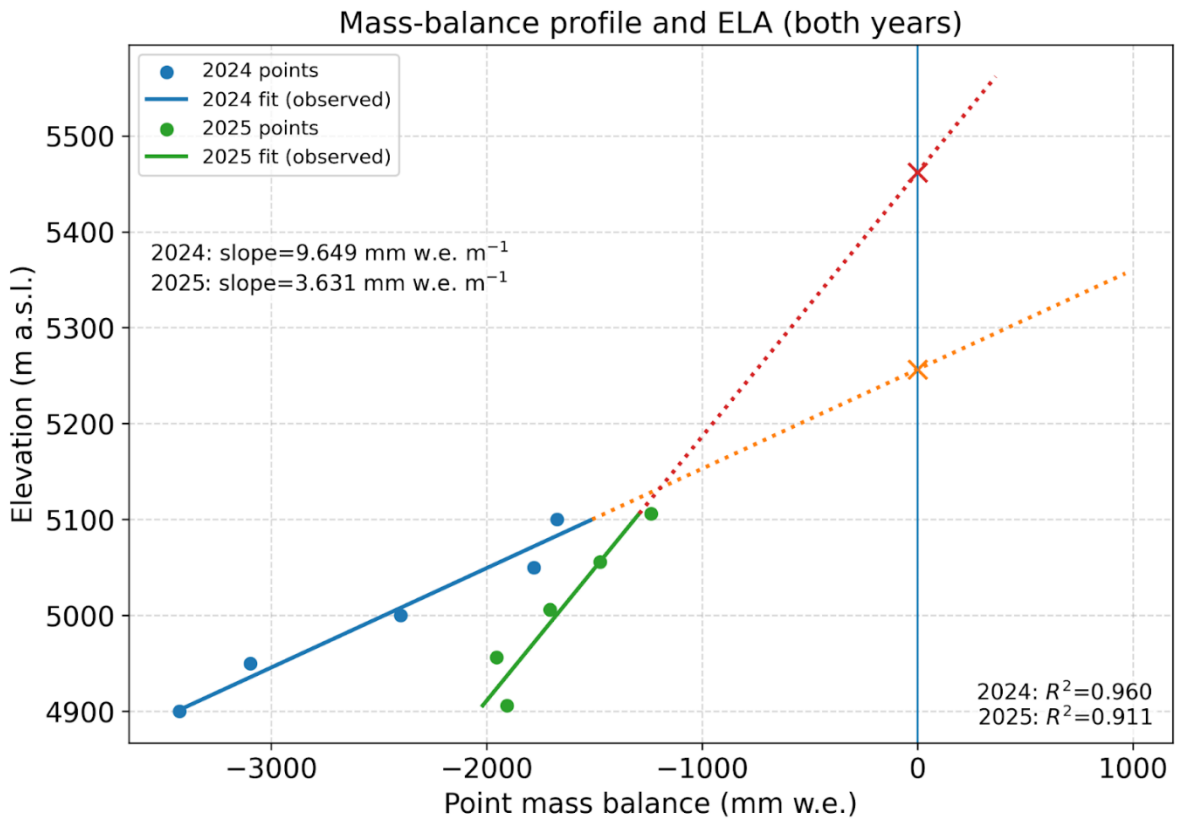

Figure 11: Equilibrium-line altitude (ELA) for 2024 and 2025.Observed point mass balance (mm w.e.) versus elevation (m a.s.l.), with solid line as linear fit and dotted line showing extrapolation

6.6 Implications for long-term glacier evolution and water resources

The combined evidence of strong negative mass balance, surface thinning, area reduction, shifting of ELA to higher elevation and terminus retreat suggests that Gangju La Glacier remains highly sensitive to ongoing climatic warming. Continued mass loss implies a progressive reduction in ice volume and long-term water storage capacity, with implications for seasonal runoff and downstream hydrological regimes. These results reinforce the importance of sustained, field-based monitoring of Bhutan's benchmark glaciers to quantify future changes and support climate adaptation and water-resource planning.

7. Conclusion

This study presents a comprehensive assessment of recent changes in Gangju La Glacier based on in-situ geodetic measurements for the 2024–2025 glaciological year, supported by longer-term geometric observations. The area averaged annual specific mass balance of −1613.876 ± 236.482 mm w.e. a^{-1} confirms continued and substantial mass loss, extending the record of persistent negative mass balance observed at this benchmark glacier. Consistent with this, the mass-balance profile indicates that the equilibrium-line altitude (ELA) lay above the glacier surface in both years (ELA ≈ 5281.5 m a.s.l. in 2024 and 5480.8 m a.s.l. in 2025), implying an ablation-dominated regime during the survey periods.

Elevation-band analysis reveals a pronounced elevation-dependent thinning pattern, with stronger surface lowering at lower elevations and reduced thinning toward higher elevations. Although the most negative thinning occurs near the glacier tongue, the mid-elevation zone exerts the greatest control on the area averaged mass balance due to its large areal extent, highlighting the critical role of glacier hypsometry in determining integrated mass-balance responses. Overall, the persistence of negative balances across the observed elevation range indicates that unfavorable climatic forcing affected the glacier broadly during the measurement period.

In addition to vertical thinning, Gangju La Glacier has undergone significant geometric changes. Glacier area decreased from 0.237 km² in 2017 to 0.169 km² in 2025, representing a loss of approximately 28.7% of its surface area. Over longer timescales, cumulative terminus mapping from 2004 to 2025 reveals persistent frontal retreat, with the most recent survey period recording a mean terminus recession of 11.86 m. The concurrence of surface lowering, area shrinkage, and terminus retreat provides clear geometric evidence of ongoing glacier recession.

Together, these findings indicate that Gangju La Glacier remains highly sensitive to ongoing climatic warming and is likely to continue losing mass under current conditions. Continued glacier degradation implies a progressive reduction in long-term ice storage and potential changes in seasonal runoff, with implications for downstream water availability and hazard risk. The results underscore the importance of sustained, field-based monitoring of Bhutan's benchmark glaciers to strengthen national cryosphere records, support hydrological assessments, and inform climate adaptation and water-resource management strategies in the eastern Himalaya.

8. References

Barry, R. G. (2006). The status of research on glaciers and global glacier recession: A review. Progress in Physical Geography: Earth and Environment, 30(3), 285–306. https://doi.org/10.1191/0309133306pp478ra

Immerzeel, W. W., Van Beek, L. P. H., & Bierkens, M. F. P. (2010). Climate change will affect the Asian water towers. Science, 328(5984), 1382–1385. https://doi.org/10.1126/science.1183188

Intergovernmental Panel on Climate Change (IPCC). (2023). Climate change 2023: Synthesis report. Contribution of Working Groups I, II and III to the Sixth Assessment Report of the Intergovernmental Panel on Climate Change. https://www.ipcc.ch/report/sixth-assessment-report-cycle/

King, O., Bhattacharya, A., Bhambri, R., & Bolch, T. (2019). Glacial lakes exacerbate Himalayan glacier mass loss. *Scientific Reports*, 9(1), 1–9. https://doi.org/10.1038/s41598-019-53733-x

Kraaijenbrink, P. D. A., Bierkens, M. F. P., Lutz, A. F., & Immerzeel, W. W. (2017). Impact of a global temperature rise of 1.5 °C on Asia's glaciers. *Nature*, 549(7671), 257–260. https://doi.org/10.1038/nature23878

National Center for Hydrology and Meteorology. (2018). *Bhutan glacier inventory 2018*. Royal Government of Bhutan. ISBN: 978-99980-862-2-7

National Center for Hydrology and Meteorology. (2024). *Annual report 2023–2024*. Royal Government of Bhutan.

Tshering, P., & Fujita, K. (2016). First in situ record of decadal glacier mass balance (2003–2014) from the Bhutan Himalaya. *Annals of Glaciology*, 57(71), 289–294. https://doi.org/10.3189/2016aog71a036

National Center for Hydrology and Meteorology. (2019). *Technical report on Gangju La Glacier: September–October 2019* (Technical report). National Center for Hydrology and Meteorology, Royal Government of Bhutan. Retrieved from

https://www.nchm.gov.bt/attachment/ckfinder/userfiles/files/Technical%20Report%20on%20Gangju%20La%20GLacier%20_%20september%20-October%202019.pdf

National Center for Hydrology and Meteorology. (2024). *Glacier mass balance studies on Gangju La 2023–2024* (Technical Report). National Center for Hydrology and Meteorology, Royal Government of Bhutan. Retrieved from https://www.nchm.gov.bt/attachment/ckfinder/userfiles/files/Gangju%20LA_Tech_2024.pdf

Brun, F., Berthier, E., Wagnon, P., Kääb, A., & Treichler, D. (2017). A spatially resolved estimate of High Mountain Asia glacier mass balances from 2000 to 2016. *Nature Geoscience*.

Hugonnet, R., et al. (2021). Accelerated global glacier mass loss in the early twenty-first century. *Nature*.

Immerzeel, W. W., et al. (2020). Importance and vulnerability of the world's water towers. *Nature*.

Maurer, J. M., Rupper, S. B., & Schaefer, J. M. (2016). Quantifying ice loss in the eastern Himalayas since 1974 using declassified spy satellite imagery. *The Cryosphere*.

Sato, Y., et al. (2022). Land- to lake-terminating transition triggers dynamic thinning of a Bhutanese glacier. *The Cryosphere*.

Shean, D. E., et al. (2020). A systematic, regional assessment of High Mountain Asia glacier mass balance. *Frontiers in Earth Science*.

The GlaMBIE Team. (2025). Community estimate of global glacier mass changes from 2000 to 2023. *Nature*. Nature

Wangchuk, T., et al. (2024). A glacial lake outburst flood risk assessment for the Phochhu river basin, Bhutan. *Natural Hazards and Earth System Sciences*. NHESS

Bhutan Glacier Inventory (BGI). (2018). *Bhutan Glacier Inventory 2018* (NCHM report).

National Center for Hydrology and Meteorology (NCHM), Cryosphere Services Division. (2024). *Glacier Mass Balance Studies on Thana Glacier 2023–2024* (Technical report). National Center for Hydrology and Meteorology, Bhutan.

National Center for Hydrology and Meteorology (NCHM), Cryosphere Services Division. (2025). *Annual Glacier Mass Balance on Shodug Glacier 2024–2025* (Technical report). National Center for Hydrology and Meteorology, Bhutan.

Stumm, D., Joshi, S. P., Gurung, T. R., & Silwal, G. (2021). Mass balances of Yala and Rikha Samba glaciers, Nepal, from 2000 to 2017. *Earth System Science Data, 13*, 3791–3818. doi:10.5194/essd-13-3791-2021

Azam, M. F., Vincent, C., Srivastava, S., Berthier, E., Wagnon, P., Kaushik, H., Hussain, Md. A., Munda, M. K., Mandal, A., & Ramanathan, A. (2024). Reanalysis of the longest mass balance series in Himalaya using a nonlinear model: Chhota Shigri Glacier (India). *The Cryosphere, 18*, 5653–5672. doi:10.5194/tc-18-5653-2024

Annex A: Hypsometric elevation-band statistics and point mass balance

Table A1 summarizes elevation-band (hypsometric) elevation differences (Δh), derived areas, perimeter, and point mass balance outputs used in the geodetic mass balance workflow.

Elevation band (m a.s.l.)	Mid-elevation (m)	Pixel count	Mean Δh (m)	Mean band area (m²)	Area (%)	Perimeter (m)	Point mass balance (mm w.e.)	Area-weighted MB contribution (mm w.e.)	Uncertainty (Ice)	Uncertainty (Snow)
[4881,4931]	4906	722	-2.165	13,772.5	8.12	349.942	-1904.94	-154.671	19.279	-
[4931,4981]	4956	883	-2.221	26,189.5	15.44	281.564	-1954.61	-301.789	36.112	-
[4981,5031]	5006	971	-1.938	39,921.0	23.54	394.553	-1705.43	-401.376	55.457	-
[5031,5081]	5056	1693	-1.674	72,837.5	42.94	595.475	-1473.42	-632.700	103.216	-
[5081,5131]	5106	368	-1.407	16,902.5	9.96	504.768	-1237.7	-123.340	22.418	-

Summary statistics:

- Total Area Average: 169623.0 m^2
- Total Uncertainty Ice: 236.482
- Total Uncertainty Snow: _
- Overall Uncertainty Average: 236.482
- Area wide mass balance: -1613.876 mm w.e.a^{-1}

Annex B: Physical Assumptions

Densities used

The following densities were applied for the geodetic mass balance measurement:

- **Ice density:** $\rho_i \approx 880$ kg m^{-3}
- **Snow density:** $\rho_s \approx 400$ kg m^{-3}
- **Water density:** $\rho_w \approx 1000$ kg m^{-3}

Annex C: Unit equivalence used in mass-balance calculations

Unit equivalence (kg m^{-2} to mm w.e.)

In glacier mass-balance studies, mass changes are commonly expressed either as mass per unit area (kg m^{-2}) or as millimeters of water equivalent (mm w.e.). These two units are directly and numerically equivalent due to the physical relationship between mass, area, thickness, and the density of liquid water.

Mass balance expressed in kg m^{-2} represents the amount of mass gained or lost per square meter of glacier surface. When this mass is converted to an equivalent thickness of water, the relationship is given by:

$$h = \frac{m}{\rho_w}$$

where

h= equivalent water thickness (m),

m= mass per unit area (kg m^{-2}), and

ρ_w= density of liquid water (≈ 1000 kg m^{-3}).

For a mass change of 1 kg m^{-2}:

$$h = \frac{1 \text{ kg m}^{-2}}{1000 \text{ kg m}^{-3}} = 0.001 \text{ m} = 1 \text{ mm}$$

Thus, a mass of 1 kg uniformly distributed over an area of 1 m² corresponds to a water layer of 1 mm thickness. This leads to the direct numerical equivalence:

$$1 \text{ kg m}^{-2} = 1 \text{ mm w.e.}$$

As a result, glacier mass-balance values reported in kg m^{-2} can be directly expressed in millimeters of water equivalent without further scaling, provided the reference density is that of liquid water. This convention allows glacier mass changes to be interpreted intuitively as an equivalent water depth and facilitates comparison across glaciers of different sizes.

Annex D: Snow and ice density uncertainty in mass-balance calculations

In the conversion of elevation change to mass balance, assumed densities for glacier ice and snow introduce an additional source of uncertainty. These densities are not constant; they vary spatially and temporally due to differences in internal structure, compaction, temperature, and metamorphic processes. To account for this variability, density-related uncertainties were explicitly included in the uncertainty propagation. Reference densities for glacier ice and snow were adopted as specified in Annex C. Based on commonly reported ranges in glaciological studies, density uncertainties of ±30 kg m^{-3} for ice and ±100 kg m^{-3} for snow were applied. The smaller uncertainty for ice reflects its relatively stable physical properties, whereas the larger uncertainty for snow accounts for its high natural variability associated with accumulation conditions,

compaction, and melt processes. However, for the current study, no snow was observed during the two consecutive mass-balance survey periods. Therefore, only the density uncertainty associated with glacier ice was considered in the final uncertainty calculation.